CHORUS

This is the accepted manuscript made available via CHORUS. The article has been published as:

# Nonlinear conductance in nanoscale CoFeB/MgO magnetic tunnel junctions with perpendicular easy axis

Motoya Shinozaki, Junta Igarashi, Shuichi Iwakiri, Takahito Kitada, Keisuke Hayakawa, Butsurin Jinnai, Tomohiro Otsuka, Shunsuke Fukami, Kensuke Kobayashi, and Hideo Ohno

Phys. Rev. B **107**, 094436 — Published 30 March 2023

DOI: 10.1103/PhysRevB.107.094436

# Nonlinear conductance in nanoscale CoFeB/MgO magnetic tunnel junctions with perpendicular easy axis

Motoya Shinozaki,[1,2] Junta Igarashi,[1,3] Shuichi Iwakiri,[4] Takahito Kitada,[1,2] Keisuke Hayakawa,[1,2] Butsurin Jinnai,[5] Tomohiro Otsuka,[1,2,5,6,7,*] Shunsuke Fukami,[1,2,5,6,8,9,†] Kensuke Kobayashi,[10,11] and Hideo Ohno[1,2,5,6,8]

*[1]Research Institute of Electrical Communication, Tohoku University, 2-1-1 Katahira, Aoba-ku, Sendai 980-8577, Japan*

*[2]Graduate School of Engineering, Tohoku University, 468-1 Aramaki Aza Aoba, Aoba-ku, Sendai 980-0845, Japan*

*[3]Université de Lorraine, Institut Jean Lamour, UMR CNRS 7198, Nancy, France*

*[4]Solid State Physics Laboratory, ETH Zürich, CH-8093 Zürich, Switzerland*

*[5]WPI-Advanced Institute for Materials Research, Tohoku University, 2-1-1 Katahira, Aoba-ku, Sendai 980–8577, Japan*

*[6]Center for Science and Innovation in Spintronics, Tohoku University, 2-1-1 Katahira, Aoba-ku, Sendai 980-8577, Japan*

*[7]Center for Emergent Matter Science, RIKEN, 2-1 Hirosawa, Wako, Saitama 351-0198, Japan*

*[8]Center for Innovative Integrated Electronic Systems, Tohoku University, 468-1 Aramaki Aza Aoba, Aoba-ku, Sendai 980–0845, Japan*

*[9]Inamori Research Institute of Science, Kyoto 600-8411, Japan*

*[10]Institute for Physics of Intelligence (IPI) & Department of Physics, Graduate School of Science, The University of Tokyo, Bunkyo, Tokyo 113-0033, Japan*

*[11]Trans-scale Quantum Science Institute, The University of Tokyo, Bunkyo, Tokyo 113-0033, Japan*

(Dated: February 21, 2023)

## Abstract

Magnetic tunnel junction (MTJ) exhibits spin-dependent conductance that governs its performance in various applications. While the transport characteristics are known to show nonlinearity, its behavior and underlying mechanism have not yet understood well. Here we investigate the nonlinear conductance at a low bias regime in nanoscale MTJs with a perpendicular magnetic easy axis and various junction sizes, by measuring current-voltage ($IV$) characteristics and ferromagnetic resonance. We evaluate $IV$ properties as $I = G_1V + G_2V^2 + G_3V^3$ under various external magnetic fields and examine the correlation between $G_1$, $G_2$ and $G_3$. We find that $G_2$ increases with decreasing the junction size, $G_3$ has a negative correlation with $G_1$, and $\delta G_3/\delta G_1$ $(= k)$ has a positive correlation with $G_2$. These results can be explained by considering the spin-flip during the tunneling and a modulation of material properties at the device edge caused by the nanofabrication process. Ferromagnetic resonance measurement supports the physical picture suggested by the transport measurements. Our finding sheds light on the mechanism of electron transport in nanoscale MTJs and facilitates the establishment of a rigorous model describing their nonlinear conductance.

## I. INTRODUCTION

A variety of quantum mechanical effects are observed in mesoscopic systems, including the tunneling effect of electrons passing through a potential barrier. Tunnel junctions based on this effect have been well studied and various attractive physical phenomena have been revealed such as the Esaki diode [1] and the Josephson effect [2]. Magnetic tunnel junction (MTJ) consisting of ferromagnet/insulator/ferromagnet structure is a typical example of a tunneling device, exhibiting spin-dependent tunneling conduction [3–5]. The resistance of the MTJ depends on the relative magnetization angle between the two ferromagnetic layers, known as the tunneling magnetoresistance (TMR) effect. Obtaining a large TMR effect is crucial for various applications such as nonvolatile memory [6–9], magnetic sensor [10], and high-frequency devices [11, 12]. The TMR effect is known to be suppressed at finite bias voltage because of its nonlinear current-voltage ($IV$) characteristics [13, 14]. Therefore, it is important to understand the nonlinear $IV$ characteristics in MTJs. The nonlinear conductance can be represented as a polynomial expansion of $IV$ characteristics at a low bias regime as

$$I = G_1 V + G_2 V^2 + G_3 V^3 + \cdots . \tag{1}$$

Tunnel junctions in general have a built-in nonlinear conductance originating from a modulation of the barrier height due to the bias voltage, which is well described by the Simmons [15] and Brinkman [16] models based on the WKB approximation. These models anticipate a positive correlation between the linear and third-order nonlinear conductance ($G_1$ and $G_3$), and this relationship has been used to quantify the barrier height [14, 17–19]. On the contrary, a recent experiment on hundreds-nm scale elliptic CoFeB/MgO MTJs with an in-plane magnetic easy axis observed a negative correlation between them [20] at a low bias regime and explained it by a phenomenological model based on the Jullire model considering a magnon-assisted tunneling [13, 14, 20–26]. However, such an experimental report is limited, and inspection of a wider variety MTJs promises to elucidate the universal mechanism of nonlinear spin-dependent transport. Since nanoscale MTJs with a perpendicular easy axis have attracted much attention from both fundamental and technological aspects [6–9], it is of great interest to investigate the nonlinear transport properties of such MTJs. In addition, the tunneling electrons in MTJs are accompanied by flows of spin-angular momentum as well as the electric charge in MTJs, leading to a spin-transfer torque, a reciprocal effect of TMR, that can be evaluated by a spin-torque ferromagnetic resonance (ST-FMR) [27]. Accordingly, comprehensive characterization based on $IV$ and ST-FMR measurements should shed light

on the mechanism of electron transport in MTJs.

Here we investigate the nonlinear electron transport in nanoscale CoFeB/MgO MTJs with a perpendicular magnetic easy axis below the junction size of 100 nm [6], which are relevant for nonvolatile memory application [6–9]. In addition to the transport properties, ST-FMR is measured to evaluate the spin-transfer torque reflecting the spin-polarized current. We show the variation of the linear ($G_1$), the second-order ($G_2$) and the third-order ($G_3$) nonlinear conductance as well as the ST-FMR spectra with the junction size ranging from 15 to 100 nm. The obtained size dependence and the correlation between each parameter are discussed by considering the modulation of the band structure at the device edge and an electron-magnon interaction.

## II. CURRENT-VOLTAGE CHARACTERISTICS

### A. Experimental setup

A stack from the substrate side, Ta (5 nm)/Pt (5 nm)/[Co (0.4 nm)/Pt (0.4 nm)]$_6$/Co (0.4 nm)/Ru (0.4 nm)/[Co (0.4 nm)/Pt (0.4 nm)]$_2$/Co (0.4 nm)/Ta (0.2 nm)/$(Co_{0.25}Fe_{0.75})_{75}B_{25}$ (1 nm)/MgO (1.2 nm)/$(Co_{0.25}Fe_{0.75})_{75}B_{25}$ (1.8 nm)/Ta (5 nm)/ Ru (5 nm) is deposited by dc/rf magnetron sputtering on a thermally oxidized Si substrate. The numbers in parentheses are nominal thicknesses. The top CoFeB (1.8 nm) corresponds to the free layer whereas the layers beneath MgO corresponds to the reference layer with a synthetic ferrimagnetic structure consisting of two Co/Pt multilayers separated by the Ru layer. Both the free and reference layers have a perpendicular easy axis.

The stack is processed into circular MTJs with various diameters $D$ ranging from 15 to 100 nm by electron beam lithography, reactive ion etching, and Ar ion milling. After processing, MTJs are annealed at 300°C for 1 h. Diameters of MTJs are electrically determined from the resistance ($R$) of the parallel state and a separately determined resistance-area ($A$) product ($RA = 12\,\Omega\mu\mathrm{m}^2$). Figure 1(a) shows the measurement setup for $IV$ characteristics. In-plane magnetic field $H_{\mathrm{in}}$ is applied to tune the tilt angle of the free-layer magnetization, leading to a continuous change in conductance. A hysteresis loop is observed in Fig. 1(b) probably due to a slight perpendicular component of the applied field by a misalignment of the electromagnet [28]. TMR ratio of about 100% is obtained for all the devices studied here. Current $I$ is measured while varying the voltage input $V$ under various $H_{\mathrm{in}}$. In the following, we focus on the $IV$ characteristics in the negative field ranging from -310 to -10 mT (shown by red plots), where a larger modulation of the conductance is

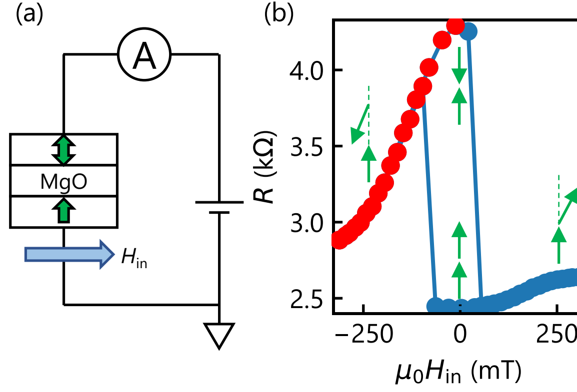


FIG. 1: (a) Measurement setup for the $IV$ characteristics. The in-plane magnetic field $H_{\rm in}$ is applied. (b) Typical $RH_{\rm in}$ curve for $D$ = 80 nm. Resistance is determined from current at bias voltage of 5 mV. The green arrows indicate possible magnetization configurations of the free and reference layers. Red plots represent the region where $IV$ measurement is performed to evaluate the nonlinear conductance.

observed compared with the positive field range. Major and minor $RH$ loops under out-of-plane magnetic fields for a device with essentially the same stack structure and the same fabrication process were reported elsewhere [29].

### B. Second-order nonlinear conductance

We measure the $IV$ characteristics under various $H_{\rm in}$ as shown in Fig. 2(a). Fitting Eq. 1 to the results yields ($G_1$, $G_2$, $G_3$) at each $H_{\rm in}$. Figure 2(b) show the $H_{\rm in}$ dependence of ($G_1$, $G_2$, $G_3$). $G_1$ increases with increasing $|H_{\rm in}|$ due to the TMR effect. This behavior is consistent with the $RH_{\rm in}$ curve shown in Fig. 1(b) because $G_1$ is the inverse of resistance. In contrast, $G_3$ decreases as reported in a previous study [20]. The contribution of $G_2$ to the current is much smaller than those from $G_1$ and $G_3$ terms, and shows a finite $H_{\rm in}$ dependence, whose reason is not clear but presumably be related to some factor which is not considered in the Brinkman model such as a spin-dependent coherent tunneling.

At first, we focus on $G_1$ and $G_2$ in this section. According to the Brinkman model [16], the conductance $G$ normalized by the junction area of the tunnel junction in the low bias voltage region

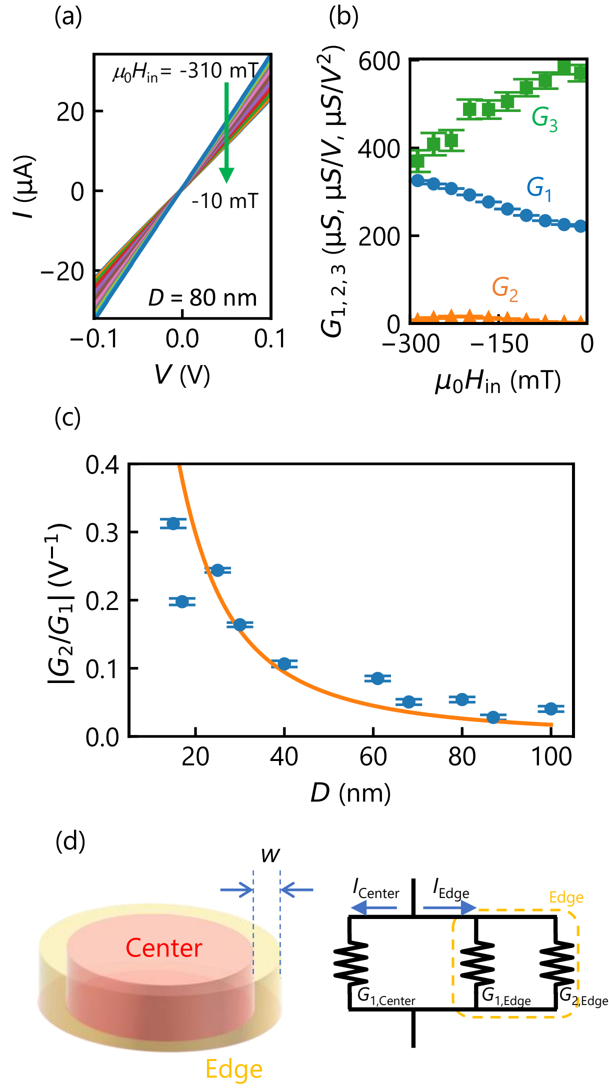


FIG. 2: (a) The $IV$ characteristics for $D$ = 80 nm under various $H_{\text{in}}$. (b) The $H_{\text{in}}$ dependence of the linear and non-linear conductance. (c) The junction size $D$ dependence of $\left|\frac{G_2}{G_1}\right|$. Plots are experimental data and the orange solid line indicates the calculation by Brinkman model [16] considering the edge effect. (d) Schematic illustration and equivalent circuit for the non-linear conductance of MTJ.

is expressed as a polynomial expansion as

$$\frac{G}{G_1} = 1 - \left(\frac{A_0 \Delta\phi}{16\phi^{\frac{3}{2}}}\right) eV + \left(\frac{9}{128}\frac{A_0^2}{\phi}\right)(eV)^2, \tag{2}$$

where, $G_1 = 3.16 \times 10^{10} \frac{\phi}{d} \exp(-1.025 d\phi^{\frac{1}{2}})$, $\phi$ is the effective barrier height at interface (electrode/insulator), $\Delta\phi$ the difference of $\phi$ between the top and bottom interfaces, $e$ the elementary

charge, $d$ the thickness (in unit of Å) of the insulator layer, and $A_0 = \frac{4(2m_\mathrm{e})^{\frac{1}{2}}d}{3\hbar}$ ($m_\mathrm{e}$ is the electron mass and $\hbar$ the Dirac's constant). In case of the MTJs with symmetric material structure such like our stack (CoFeB/MgO/CoFeB), symmetric electron transport with respect to the positive and negative biases is expected, i.e., $\Delta\phi$ and thus $G_2$ should be zero. Contrary to this expectation, however, a finite $G_2$ is observed in Fig. 2(b). Note that $G_2$ turns out to have its origin in the MTJ itself because the sign of $G_2$ is reversed when the contact probes are reversed.

To investigate the origin of $G_2$, we evaluate the $D$ dependence of $G_2$. Here, as $G_2$ changes with $H_\mathrm{in}$ as shown in Fig. 2(b), we take its maximum value for each $D$. Also, since $G_2$ has a dimension of conductance/voltage (S/V), where conductance itself depends on $D$, we use $\left|\frac{G_2}{G_1}\right|$ instead of $G_2$, so that the $D$ dependence of conductance can be canceled out, leading to an intrinsic $D$ dependence of $G_2$. $D$ dependence of $\left|\frac{G_2}{G_1}\right|$ is summarized in Fig. 2(c). One can see that $\left|\frac{G_2}{G_1}\right|$ increases with decreasing $D$. According to previous findings [30–35], such size dependence can be attributed to a modulation of material properties at the device edge due to the fabrication process, and the so-called edge effect appears more significantly in smaller $D$. Figure 2(d) shows a schematic and equivalent circuit model. The center region has a symmetric band structure, i.e., $\Delta\phi = 0$ and $G_{2,\mathrm{Center}} = 0$, whereas the edge region has an asymmetric band structure, i.e., $\Delta\phi \neq 0$ and $G_{2,\mathrm{Edge}} \neq 0$, considering the fact that the free layer is exposed to ion milling for a longer time than the reference layer [36]. As a result, $I_\mathrm{Center} = G_{1,\mathrm{Center}}V$ and $I_\mathrm{Edge} = G_{1,\mathrm{Edge}}V + G_{2,\mathrm{Edge}}V^2$ flow in the center and edge regions, respectively. Using this model with the edge width $w$ = 3 nm, $\phi$ = 0.6 eV, and $\frac{\Delta\phi}{\phi} = 0.3$, based on the literatures [19, 32–35], $\left|\frac{G_2}{G_1}\right|$ is obtained from Eq. (2) as $\frac{A_0\Delta\phi}{4\phi^{\frac{3}{2}}}\frac{w(D-w)}{D^2}$, which is shown by the orange solid curve in Fig. 2(c). The curve describes the experimental results well, indicating the validity of the model. This scenario will be supported by the FMR measurement described later.

### C. Third-order nonlinear conductance

We then investigate the third-order nonlinear conductance $G_3$. We obtain many pairs of $G_1$ and $G_3$ under various $H_\mathrm{in}$. Figure 3(a) shows the correlation between $G_3$ and $G_1$ for several junctions with different $D$. According to the Julliere model with a spin flip during the tunneling, the relationship is described by [20]

$$G_3 = -kG_1 + m, \tag{3}$$

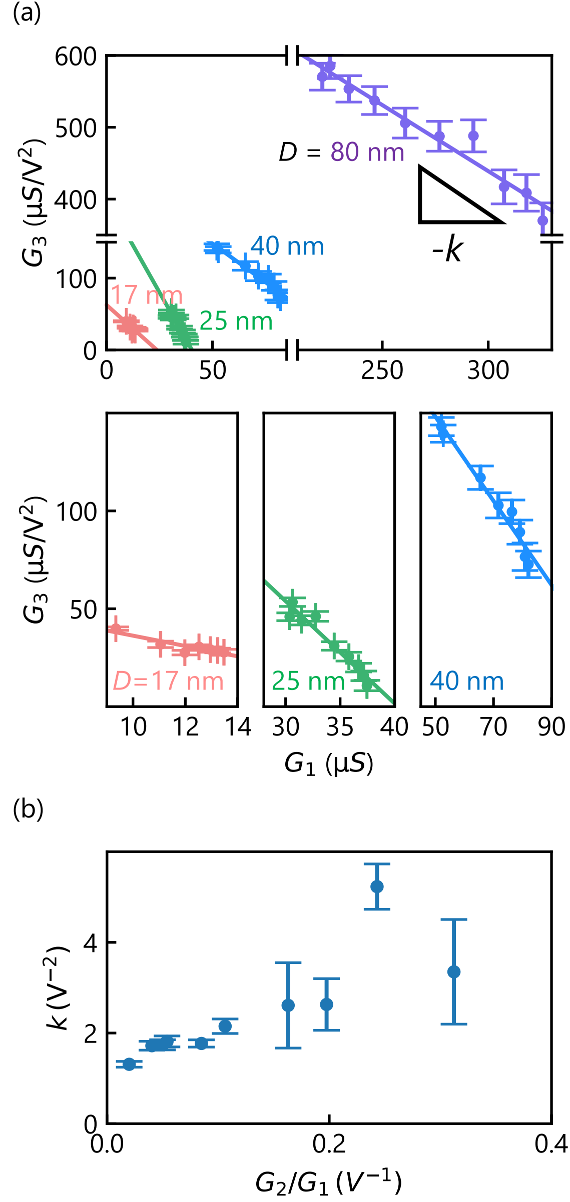


FIG. 3: (a) Correlation between $G_3$ and $G_1$ for $D = 20$, 25, 40, and 80 nm. $k$ represents the slope obtained by a linear fitting.. (b) Correlation between k and $G_2$ to $G_1$ ratio.

where $k(>0)$ $(= \delta G_3/\delta G_1 > 0)$ is a coefficient for the ratio of $G_3$ to $G_1$ and $m$ the intercept depending on the thickness of the insulator and temperature. This equation well described the experimental results for MTJs with in-plane magnetic easy axis and the slope $k$ was reported to be almost constant to be about 2 with various MgO thicknesses and temperatures [20]. Clearly seen in our results, the negative correlation between $G_3$ and $G_1$ is also observed in our MTJs and the

$k$ value is comparable with the previous report although the easy-axis direction and junction sizes are different. In addition, $k$ appears to increase with decreasing $D$ in the present study, implying the manifestation of the edge effect in $G_3$ as well as $G_2$. To examine this speculation, we plot the relationship between $k$ and $\left|\frac{G_2}{G_1}\right|$ in Fig. 3(b). Positive correlation is observed with $k \sim 2\ V^{-2}$ at $\left|\frac{G_2}{G_1}\right| \leq 0.1$, this value agrees well with the previous work with negligible $G_2$ [20] despite the different easy axis directions. We note that the data for $\left|\frac{G_2}{G_1}\right| > 0.1$ are obtained from devices with $D < 30$ nm and in such small devices experimental inaccuracy significantly increases, leading to a larger scattering of the data. Overall, the obtained result supports the speculation that the edge effect also affects $G_3$ of nanoscale MTJs as in $G_2$. We also note that consideration of an asymmetric spin polarization between free and reference layers cannot explain the variation of $k$ although it could modulate the intercept $m$ [Appendix A].

Now we discuss the origin of $G_3$ based on the results of $IV$ measurements. The negative correlation between $G_3$ with $G_1$ can be understood from the Julliere model considering the spin-flip process as described in previous studies, and this work clarifies that the mechanism is universal regardless of the magnetic easy axis direction. The magnon-assisted tunneling has been theoretically proposed as a possible scenario for the spin-flip process causing the nonlinearity [25], and this can consistently explain our experimental results. In addition, we newly find out from $\left|\frac{G_2}{G_1}\right|$ vs. $D$ and $k$ vs. $\left|\frac{G_2}{G_1}\right|$ that the edge effect also affects $G_3$. This implies that spin flip is more likely to take place near the edge, probably due to the modulated magnetic properties. Thus, rigorous theoretical model including the spatial variation of asymmetric band structure and spin flip process is expected to comprehensively describe the nonlinear conductance of nanoscale MTJs.

## III. SPIN-TORQUE FERROMAGNETIC RESONANCE

In this section, we study the ST-FMR [27], with which the current induced spin-torque reflecting the energy band structure can be evaluated, and thus the insight obtained from the nonlinear conductance can be examined from a different way.

### A. Experimental setup

Here we use the following stack deposited on a sapphire substrate: from the substrate side, Ta (5 nm)/PtMn (20 nm)/Co (2.6 nm)/Ru (0.9 nm)/ $(Co_{0.25}Fe_{0.75})_{75}B_{25}$ (2.4 nm)/MgO (1.1

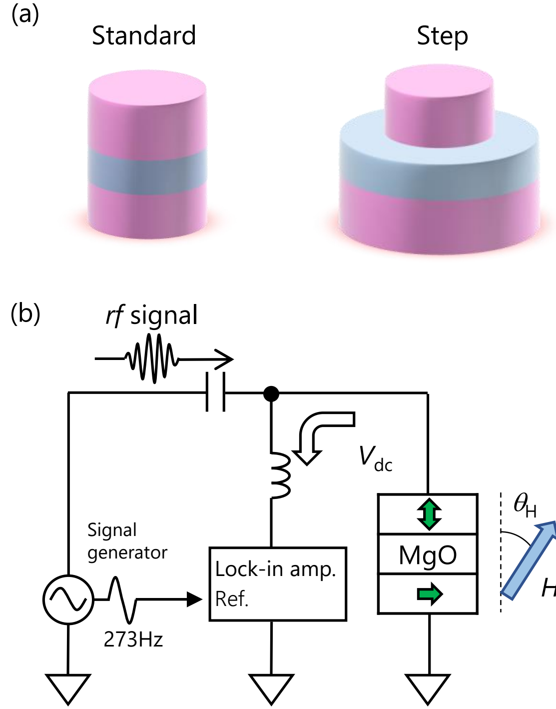


FIG. 4: (a) Illustrations of standard and step MTJ structures. (b) Measurement setup for homodyne-detected FMR. Amplitude of rf signal is modulated at 273 Hz and fixed to be -25 dBm.

nm)/$(\mathrm{Co}_{0.25}\mathrm{Fe}_{0.75})_{75}\mathrm{B}_{25}$ (1.8 nm)/Ta (5 nm)/Ru (5 nm) is deposited on a sapphire substrate. In this structure, the top free (bottom reference) layer has a perpendicular (in-plane) easy axis, allowing us to obtain FMR spectra under perpendicular magnetic field $H_{\mathrm{perp}}$ [34, 35, 37], which is beneficial for evaluating the effective fields of spin torque free from the electric-field effect as described later. We fabricate two types of MTJs shown in Fig. 4(a); one has almost the same reference layer size as that of the free layer (standard structure), and the other has the reference layer much larger than the free-layer size (step structure). The process condition for them is the same as those employed in our previous studies [32, 34, 35]. We previously found that the standard structure has a significant edge effect, whereas it is negligible in the step structure [32, 34, 35], due to the different ion-milling angles and time. We also note that the MTJs we studied in section II have the standard structure.

The measurement setup is shown in Fig. 4(b). An rf signal is applied to the MTJ through the rf port of a bias tee to induce the FMR. The MTJ resistance is synchronized with the input rf frequency during FMR, generating a rectified dc voltage via the TMR effect that can be detected

as the FMR spectrum. The amplitude of the rf signal is fixed to be -25 dBm, which is modulated at 273 Hz, and the lock-in technique is used to detect the rectified voltage through the dc port of the bias tee. We measure the spectrum for several MTJs with various free-layer diameters $D$ which is determined from $RA = 12\,\Omega\mu\mathrm{m}^2$. The FMR spectrum are measured at fixed rf frequency of 6 GHz (8 GHz only for $D$ = 33 nm of the step structure) while seeping $H_{\mathrm{perp}}$.

### B. Results

Figures 5(a) and (b) show that ST-FMR spectra of the standard and step structures, respectively, with various $D$. While a few small peaks associated with spin-wave resonance are observed [35], we focus on the largest peak associated with the uniform mode. The peak position shifts with D due to a change in shape anisotropy normal to the MTJ [28, 33, 34, 38, 39]. Also, at a glance, the spectrum shape changes from symmetric to antisymmetric below $D$ = 40 nm for the standard structure, whereas the step structure keeps symmetric shape for all $D$.

The FMR spectrum is generally described by a sum of symmetric and anti-symmetric Lorentz functions as

$$V_{\mathrm{dc}} = \frac{\Delta H}{4(H-H_{\mathrm{R}})^2+\Delta H^2}S + \frac{H_1(H^2-H_{\mathrm{R}}^2)}{(H^2-H_{\mathrm{R}}^2)+\Delta H^2}A, \tag{4}$$

where, $S$ and $A$ are the amplitude of symmetric (first term) and anti-symmetric (second term) Lorentz functions. $H$ is the external magnetic field, $H_{\mathrm{R}}$ the resonance field, $H_1$ the effective static magnetic field, and $\Delta H$ the linewidth of the FMR spectrum. By fitting Eq. 4 to the spectra, $S$, $A$, $H_{\mathrm{R}}$, $H_1$, and $\Delta H$ can be determined. The shape of FMR spectrum is known to reflect the excitation sources [27]; the symmetric component originates from the spin-transfer torque (STT) and the anti-symmetric one from the field-like torque (FLT) and an electric-field effect on magnetic anisotropy [40–42]. In this measurement configuration, we only have to consider the STT and the FLT (see Appendices B and C). In the ST-FMR, the amplitudes of spectrum, $S$ and $A$, are proportional to bias voltage derivative of the effective field, so-called torkance. The effective fields of STT and FLT are given as [43, 44]

$$a_J = \frac{\hbar}{2e}\frac{g(\theta)}{M_{\mathrm{S}}t}J, \tag{5}$$

$$b_J = C_1 V + C_2 V^2, \tag{6}$$

leading to the expression of FLT torkance as

$$\frac{\mathrm{d}b_J}{\mathrm{d}V} = C_1 + 2C_2V, \tag{7}$$

where $e$ is the elementary charge, $g(\theta)$ a spin-transfer efficiency, $\theta$ the relative angle between the magnetization of free and reference layer, $M_\mathrm{S}$ the spontaneous magnetization, $t$ the effective thickness of the free layer, and $V$ the bias voltage. In MTJs with symmetric band structure, only $C_2$ component should be finite, whereas the linear response term $C_1$ could appear according to the scattering theory considering the asymmetric band structure [44–47]. Equation (7) indicates that the amplitude of antisymmetric component $A$ of FMR spectrum at $V = 0$ signifies the presence of ($A \propto \frac{\mathrm{d}b_J}{\mathrm{d}V}\big|_{V=0} = C_1$) [46, 47].

Based on this prior knowledge, now we discuss the implication of the results shown in Fig. 5 in conjunction with the findings from the $IV$ characteristics. Even though the MTJ we study has a symmetric material structure (CoFeB (free)/MgO/CoFeB (ref.)) predicting $C_1 = 0$, the antisymmetric component appears with decreasing $D$ for the standard structure, whereas it is not the case for the step structure. Considering the previous findings that the edge effect is significant (negligible) in the standard (step) structure, this observation indicates that, for the step structure, the band structure is symmetric and spatially uniform. In contrast, the standard structure is symmetric (asymmetric) in the center (edge) region as depicted in Fig. 2(d), supporting our scenario deduced from the results of nonlinear conductance. We finally note that while our MTJs have a reference layer with a synthetic ferrimagnetic structure, its effect on the asymmetry of band structure should be minor compared to the effect of fabrication process because the symmetric FMR spectra is observed for the step structure at all $D$.

## IV. CONCLUSION

In conclusion, we investigate the nonlinear conductance at a low bias regime in nanoscale MTJs with a perpendicular magnetic easy axis. Finite second-order nonlinear conductance $G_2$ is observed despite the employment of the same material for the free and the reference layers, and it increases with decreasing the device size. This result is explained by a model considering an asymmetric band structure near the device edge due to the edge effect caused by the fabrication process, and the model is supported by a ST-FMR measurement. We also observe a negative correlation between the linear conductance $G_1$ and the third-order nonlinear conductance $G_3$ as

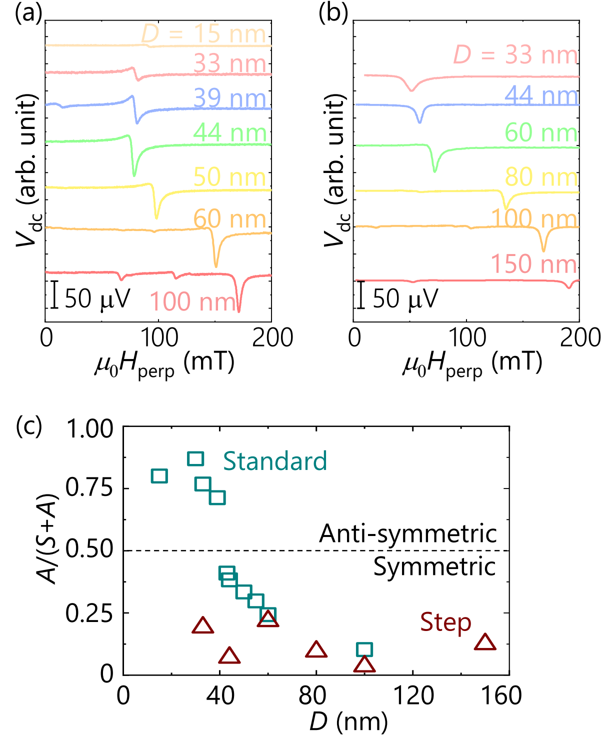


FIG. 5: (a) Free-layer size $D$ dependence of FMR spectra for (a) standard and (b) step structures. (c) $D$ dependence of the anti-symmetric component of the FMR spectrum. Square and triangle symbols correspond to the standard and step structures, respectively.

in a previous work on an in-plane easy-axis MTJs, and the slope for the negative correlation $k$ is comparable with the reported value. This result indicates a generality of the mechanism governing $G_3$ of MTJ, *e.g.,* a spin-flip during the tunneling. Our findings also show that the nonlinear transport model considering the spin-flip tunneling holds true even in a presence of an additional term such as $G_2$, and this is an advanced finding firmly illustrating the generality of the phenomena. Furthermore, the $k$ shows a positive correlation with $\left|\frac{G_2}{G_1}\right|$. These results imply that the asymmetry of the band structure modulates not only $G_2$ but also $G_3$. This study sheds light on the origin of nonlinear conductance of MTJs, leading to a deep understanding on the non-equilibrium physics in spin-dependent systems and development of high-performance nanoscale MTJs.

## ACKNOWLEDGEMENTS

The authors thank H. Sato, and A. Okada, I. Morita, R. Ono, and M. Musya for fruitful discussion and technical support. Part of this work is supported by JST-OPERA (No. JPMJOP1611), JST-PRESTO (JPMJPR16N3), MEXT Leading Initiative for Excellent Young Researchers, Grants-in-Aid for Scientific Research from JSPS (Nos. 21K18592, 20H00237, 20J14418, 19H05622, 19H05826, 19H00656), MEXT Initiative to Establish Next-generation Novel Integrated Circuits Centers (X-NICS) Grant Number JPJ011438, Hattori Hokokai Foundation Research Grant, Kondo Zaidan Research Grant, FRiD Tohoku University, and Cooperative Research Projects of RIEC. M.S. acknowledges financial support from JST-OPERA and DIARE of Tohoku University.

## APPENDIX A: EFFECT OF SPIN POLARIZATION ASYMMETRY ON NONLINEAR CONDUCTANCE

Here, we extend the Julliere model with the magnon-assisted tunneling to include the asymmetry of spin polarization. Spin polarization of the free (reference) layers $p_{\mathrm{F(R)}}$ are introduced as

$$p_{\mathrm{F}} = \left| \frac{D^{\mathrm{F}}_{\uparrow} - D^{\mathrm{F}}_{\downarrow}}{D^{\mathrm{F}}_{\uparrow} + D^{\mathrm{F}}_{\downarrow}} \right|_{\theta_{\mathrm{F}}=0}, \tag{8}$$

$$p_{\mathrm{R}} = \left| \frac{D^{\mathrm{R}}_{\uparrow} - D^{\mathrm{R}}_{\downarrow}}{D^{\mathrm{R}}_{\uparrow} + D^{\mathrm{R}}_{\downarrow}} \right|. \tag{9}$$

Here, $D^{\mathrm{F,(R)}}_{\uparrow,\downarrow}$ is the spin-dependent density of state at the Fermi level($\uparrow$ and $\downarrow$ indicate spin up and down, respectively). The $G_1$ and $G_3$ in a asymmetrical system are described as

$$G_1 = A\tau F_D R_D \left( \frac{1 - p_{\mathrm{F}} p_{\mathrm{R}}}{2} + p_{\mathrm{F}} p_{\mathrm{R}} \cos^2 \frac{\theta}{2} \right), \tag{10}$$

$$G_3 = B\tau F_D R_D p_{\mathrm{F}} p_{\mathrm{R}} \sin^2 \frac{\theta}{2}, \tag{11}$$

where, $A$ and $B$ are the constant coefficients proportional to the junction area, $\tau$ the matrix element associated with the tunneling process. We define $F_D \equiv D^{\mathrm{F}}_{\uparrow} + D^{\mathrm{F}}_{\downarrow}|_{\theta_{\mathrm{F}}=0}$ and $R_D \equiv D^{\mathrm{R}}_{\uparrow} + D^{\mathrm{R}}_{\downarrow}$. We assume that the magnetization direction of the reference layer is fixed along the film normal. Therefore, $\theta_{\mathrm{F}} = 0, \pi$ corresponds to the parallel and antiparallel configurations, respectively. From

Eqs. 10 and 11, we obtain the relationship between $G_3$ and $G_1$ as

$$\begin{aligned} G_3 &= -\frac{B}{A}G_1 + \frac{B\tau F_D R_D}{2}\left(1 + p_{\mathrm{F}}p_{\mathrm{R}}\right) \\ &= \quad -kG_1 + m^*. \end{aligned} \tag{12}$$

The slope $k$ will be the same as when it is symmetric (Eq. 3), even though asymmetry is introduced. Therefore, it is reasonable to consider that the amplitude coefficient $B$ itself is modulated by device asymmetry.

## APPENDIX B: EQUATION OF THE RECTIFIED VOLTAGE

The Landau-Lifshitz Gilbert (LLG) equation including the STT, FLT. and electric-field effect is described as,

$$\begin{aligned} \frac{\partial \mathbf{m_F}}{\partial t} &= \gamma\mu_0(\mathbf{m_F} \times \mathbf{H_K^{eff}}) + \alpha\left(\mathbf{m_F} \times \frac{\mathrm{d}\mathbf{m_F}}{\mathrm{d}t}\right) \\ &+ \gamma\mu_0 a_{\mathrm{J}}\mathbf{m_F} \times (\mathbf{m_F} \times \mathbf{m_R}) + \gamma\mu_0 b_{\mathrm{J}}(\mathbf{m_F} \times \mathbf{m_R}) \\ &- \gamma\mu_0(\mathbf{m_F} \times \mathbf{h_K}), \end{aligned} \tag{13}$$

where, $\mathbf{m_F}$ and $\mathbf{m_R}$ are the unit magnetization vectors of free and reference layer, respectively. $\gamma$ is the gyromagnetic ratio, $\alpha$ the damping constant, and $\mathbf{h_K}$ the effective field of electric-effect described by the following equation:

$$\mathbf{h_K} = \begin{pmatrix} 0 \\ 0 \\ h_K \cos\theta_{\mathrm{F}} \end{pmatrix} \tag{14}$$

During the FMR, the resistance of MTJ is

$$\begin{aligned} R(t) &= \frac{2R_{\mathrm{AP}}R_{\mathrm{P}}}{R_{\mathrm{AP}} + R_{\mathrm{AP}} + (R_{\mathrm{AP}} - R_{\mathrm{P}})\cos(\theta_0 + \delta\theta\sin(\omega t))} \\ &\approx R_0 + \frac{R_0^2}{2R_{\mathrm{AP}}}\tau_{\mathrm{TMR}}\delta\theta\sin\theta_0\sin(\omega t), \end{aligned} \tag{15}$$

where $\theta_0$ is the relative angle between the magnetization of free and reference layers, $\delta\theta$ the amplitude of the precession angle, $R_0$ the equivalent resistance $R|_{\delta\theta=0}$, and $\tau_{\mathrm{TMR}}$ the tunnel magnetoresistance ratio. Hence, the rectified voltage $V_{\mathrm{dc}}$ by rf current $I_{\mathrm{rf}}\sin(\omega t)$ is

$$V_{\mathrm{dc}} \approx \frac{R_0^2 I_{\mathrm{rf}}}{4R_{\mathrm{AP}}}\tau_{\mathrm{TMR}}\delta\theta\sin\theta_0. \tag{16}$$

In case of the liner FMR region, we can treat $\delta\theta$ to Re$[\delta m_{\rm F,x}]$. Here, $\delta m_{\rm F,x}$ is the precession amplitude of $\mathbf{m_F}$ with x-axis component and can be derived from Eq. 13. Then, $a_{\rm J}$ and $b_{\rm J}$ depends on a bias current (voltage). Therefore, we should treat them by $\hat{a_{\rm J}}$ and $\hat{b_{\rm J}}$ as

$$\hat{a_{\rm J}}, \hat{b_{\rm J}} = \left.\frac{{\rm d}a_{\rm J}, b_{\rm J}}{{\rm d}I}\right|_{\rm I_{bias}} I_{\rm rf}. \tag{17}$$

Acordingly, we obtain Eq. 4 as

$$\begin{aligned} V_{\rm dc} \approx \eta \frac{R_0^2 I_{\rm rf} \tau_{\rm TMR}}{4R_{\rm AP}} \Bigg[ & \frac{\hat{a_{\rm J}} \sin^2\theta_0 \Delta H}{4(H-\Delta H_{\rm R})^2 + \Delta H^2} \\ & + \frac{H_1(H^2 - H_{\rm R}^2)}{(H^2 - \Delta H_{\rm R}^2) + (H\Delta H)^2} \Big( \hat{b_{\rm J}} \sin^2\theta_0 \\ & + h_K \sin\theta_0 \sin\theta_{\rm F} \cos\theta_{\rm F} \Big) \Bigg]. \end{aligned} \tag{18}$$

Here, $\eta$ is the transmission coefficient described as

$$\eta = \left[ 1 - \left( \frac{Z-50}{Z+50} \right)^2 \right], \tag{19}$$

where, $Z$ is the impedance of MTJ device. Under the perpendicular magnetic field, Eq. 18 can be described by sum of symmetric and anti-symmetric Lorentz functions as

$$\begin{aligned} V_{\rm dc} \approx \eta \frac{R_0^2 I_{\rm rf} \tau_{\rm TMR}}{4R_{\rm AP}} \Bigg[ & \frac{\hat{a_{\rm J}} \sin^2\theta_0 \Delta H}{4(H-\Delta H_{\rm R})^2 + \Delta H^2} \\ & + \frac{2(H - H_{\rm R})}{4(H-\Delta H_{\rm R})^2 + \Delta H^2} \Big( \hat{b_{\rm J}} \sin^2\theta_0 \\ & + h_K \sin\theta_0 \sin\theta_{\rm F} \cos\theta_{\rm F} \Big) \Bigg] \\ = & \, S L_{\rm S}(H) + A L_{\rm A}(H). \end{aligned} \tag{20}$$

Therefore, amplitudes of symmetric and anti-symmetric Lorentz functions $S$ and $A$ are proposal to the torkance of the effective fields of STT and FLT, respectively.

## APPENDIX C: EXCITATION SOURCE OF FMR

In case of $\theta_{\rm F} = 0$, electric-field effect cannot excite the uniform mode because the directions of magnetization and anisotropy modulation are parallel. However, quasi-uniform mode arisen from non-uniformity of magnetization can be excited by the electric-field effect under the perpendicular magnetic field [48–50]. The FMR spectrum excited by FLT has a different angle dependence

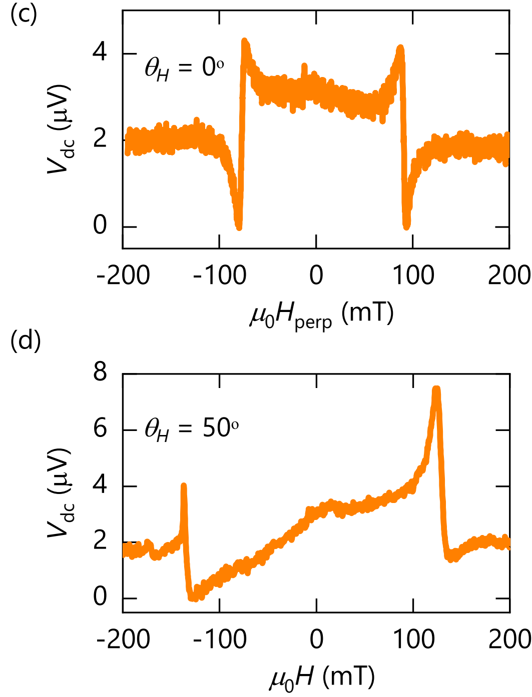


FIG. 6: The FMR spectrum of $D$ = 15 nm with (a) $\theta_H = 0°$ and (b) $50°$

compared with the one by the electric field effect. The amplitude originated from the STT and FLT are proportional to $\sin^2\theta_0$ and the electric-field effect to $\sin\theta_0 \sin\theta_\mathrm{F} \cos\theta_\mathrm{F}$ (see in Appendix B). The STT and the FLT have a maximum value at $\theta_0 = 90°$, whereas the electric field effect at $\theta_\mathrm{F} = 55°$ [42]. In order to identify the excitation sources of anti-symmetric component, we measure the FMR at the magnetic field angle of $0^{\circ}$ and $50^{\circ}$ from the perpendicular direction for a MTJ with $D$ = 15 nm and the standard structure. The results are shown in Figs. 6(a) and (b), respectively. The FMR spectrum for $\theta_H = 0^{\circ}$ [Fig 6(a)] is symmetric to the y axis, whereas the tilted magnetic field ($\theta_H = 50^{\circ}$) [Fig 6(b)] breaks the symmetry. This is because the sign of the anti-symmetric component originating from the electric-field effect is changed with the sign change of $\cos\theta_\mathrm{F}$. These results indicate that the anti-symmetric component is mainly excited by FLT in this system under $H_\mathrm{perp}$.

---

* tomohiro.otsuka@tohoku.ac.jp

† s-fukami@tohoku.ac.jp

[1] L. Esaki, Phys. Rev. **109**, 603 (1958).

[2] B. D. Josephson, Phys. Lett. **1**, 251 (1962).

[3] M. Julliere, Phys. Lett. A **54**, 225 (1975).

[4] T. Miyazaki and N. Tezuka, J. Magn. Magn. Mater. **139**, L231 (1995).

[5] J. S. Moodera, L. R. Kinder, T. M. Wong, and R. Meservey, Phys. Rev. Lett. **74**, 3273 (1995).

[6] S. Ikeda, K. Miura, H. Yamamoto, K. Mizunuma, H. Gan, M. Endo, S. Kanai, J. Hayakawa, F. Matsukura, and H. Ohno, Nat. Mater. **9**, 721 (2010).

[7] H. Ohno, T. Endoh, T. Hanyu, N. Kasai, and S. Ikeda, in *IEEE International Electron Devices Meeting (IEDM)* (IEEE, San Francisco, CA, USA, 2010), pp. 9–4.

[8] S. Bhatti, R. Sbiaa, A. Hirohata, H. Ohno, S. Fukami, and S. Piramanayagam, Materials Today **20**, 530 (2017).

[9] S. Ikegawa, F. B. Mancoff, J. Janesky, and S. Aggarwal, IEEE Trans. Electron Devices **67**, 1407 (2020).

[10] K. Shimazawa, J. Sun, N. Kasahara, K. Sato, T. Kagami, S. Saruki, O. Redon, Y. Fujita, T. Umehara, J. Syoji, et al., IEEE Trans. Magn. **37**, 1684 (2001).

[11] S. I. Kiselev, J. Sankey, I. Krivorotov, N. Emley, R. Schoelkopf, R. Buhrman, and D. Ralph, Nature **425**, 380 (2003).

[12] R. Sharma, R. Mishra, T. Ngo, Y.-X. Guo, S. Fukami, H. Sato, H. Ohno, and H. Yang, Nat. Commun **12**, 2924 (2021).

[13] S. Zhang, P. Levy, A. Marley, and S. Parkin, Phys. Rev. Lett. **79**, 3744 (1997).

[14] J. S. Moodera, J. Nowak, and R. J. van de Veerdonk, Phys. Rev. Lett. **80**, 2941 (1998).

[15] J. G. Simmons, J. Appl. Phys. **34**, 1793 (1963).

[16] W. Brinkman, R. Dynes, and J. Rowell, J. Appl. Phys. **41**, 1915 (1970).

[17] S. S. Parkin, C. Kaiser, A. Panchula, P. M. Rice, B. Hughes, M. Samant, and S.-H. Yang, Nat, Mater. **3**, 862 (2004).

[18] S. Yuasa, T. Nagahama, A. Fukushima, Y. Suzuki, and K. Ando, Nat. Mater. **3**, 868 (2004).

[19] R. Guerrero, F. Aliev, R. Villar, J. Hauch, M. Fraune, G. Güntherodt, K. Rott, H. Brückl, and G. Reiss, Appl. Phys. Lett. **87**, 042501 (2005).

[20] S. Iwakiri, S. Sugimoto, Y. Niimi, Y. Kozuka, Y. K. Takahashi, S. Kasai, and K. Kobayashi, Phys. Rev. B **103**, 245427 (2021).

[21] F. Guinea, Phys. Rev. B **58**, 9212 (1998).

[22] C. Lü, M. Wu, and X. Han, Phys. Lett. A **319**, 205 (2003).

[23] V. Drewello, J. Schmalhorst, A. Thomas, and G. Reiss, Phys. Rev. B **77**, 014440 (2008).

[24] V. Drewello, M. Schäfers, O. Schebaum, A. A. Khan, J. Münchenberger, J. Schmalhorst, G. Reiss, and A. Thomas, Phys. Rev. B **79**, 174417 (2009).

[25] S. A. Bender, R. A. Duine, and Y. Tserkovnyak, Physical Review B **99**, 024434 (2019).

[26] K. Sano, Journal of the Physical Society of Japan **90**, 125001 (2021).

[27] A. Tulapurkar, Y. Suzuki, A. Fukushima, H. Kubota, H. Maehara, K. Tsunekawa, D. Djayaprawira, N. Watanabe, and S. Yuasa, Nature **438**, 339 (2005).

[28] E. Hirayama, S. Kanai, H. Sato, F. Matsukura, and H. Ohno, J. Appl. Phys. **117**, 17B708 (2015).

[29] H. Sato, S. Ikeda, S. Fukami, H. Honjo, S. Ishikawa, M. Yamanouchi, K. Mizunuma, F. Matsukura, and H. Ohno, Jpn. J. Appl. Phys. **53**, 04EM02 (2014).

[30] J. M. Shaw, S. E. Russek, T. Thomson, M. J. Donahue, B. D. Terris, O. Hellwig, E. Dobisz, and M. L. Schneider, Phys. Rev. B **78**, 024414 (2008).

[31] O. Ozatay, P. Gowtham, K. Tan, J. Read, K. Mkhoyan, M. Thomas, G. Fuchs, P. Braganca, E. Ryan, K. Thadani, et al., Nat. Mater. **7**, 567 (2008).

[32] J. Igarashi, J. Llandro, H. Sato, F. Matsukura, and H. Ohno, Appl. Phys. Lett. **111**, 132407 (2017).

[33] L. Thomas, G. Jan, S. Le, S. Serrano-Guisan, Y.-J. Lee, H. Liu, J. Zhu, J. Iwata-Harms, R.-Y. Tong, S. Patel, et al., in *IEEE International Electron Devices Meeting (IEDM)* (IEEE, San Francisco, CA, USA, 2017), pp. 38–4.

[34] M. Shinozaki, J. Igarashi, H. Sato, and H. Ohno, Appl. Phys. Express **11**, 043001 (2018).

[35] M. Shinozaki, T. Dohi, J. Igarashi, J. Llandro, S. Fukami, H. Sato, and H. Ohno, Appl. Phys. Lett. **117**, 202404 (2020).

[36] W. Kim, J. Jeong, Y. Kim, W. Lim, J. Kim, J. Park, H. Shin, Y. Park, K. Kim, S. Park, et al., in *IEEE International Electron Devices Meeting (IEDM)*, IEEE (IEEE, San Francisco, CA, USA, 2011), pp. 24–1.

[37] M. Shinozaki, E. Hirayama, S. Kanai, H. Sato, F. Matsukura, and H. Ohno, Appl. Phys. Express **10**, 013001 (2017).

[38] K. Mizunuma, M. Yamanouchi, H. Sato, S. Ikeda, S. Kanai, F. Matsukura, and H. Ohno, Appl. Phys. Express **6**, 063002 (2013).

[39] K. Watanabe, B. Jinnai, S. Fukami, H. Sato, and H. Ohno, Nat. Commun **9**, 663 (2018).

[40] H. Kubota, A. Fukushima, K. Yakushiji, T. Nagahama, S. Yuasa, K. Ando, H. Maehara, Y. Nagamine,

K. Tsunekawa, D. D. Djayaprawira, et al., Nat. Phys. **4**, 37 (2008).

[41] J. C. Sankey, Y.-T. Cui, J. Z. Sun, J. C. Slonczewski, R. A. Buhrman, and D. C. Ralph, Nat. Phys. **4**, 67 (2008).

[42] T. Nozaki, Y. Shiota, S. Miwa, S. Murakami, F. Bonell, S. Ishibashi, H. Kubota, K. Yakushiji, T. Saruya, A. Fukushima, et al., Nat. Phys. **8**, 491 (2012).

[43] J. Sun, J. Magn. Magn. Mater. **202**, 157 (1999).

[44] J. Xiao, G. E. Bauer, and A. Brataas, Phys. Rev. B **77**, 224419 (2008).

[45] S.-C. Oh, S.-Y. Park, A. Manchon, M. Chshiev, J.-H. Han, H.-W. Lee, J.-E. Lee, K.-T. Nam, Y. Jo, Y.-C. Kong, et al., Nat. Phys. **5**, 898 (2009).

[46] R. Matsumoto, A. Chanthbouala, J. Grollier, V. Cros, A. Fert, K. Nishimura, Y. Nagamine, H. Maehara, K. Tsunekawa, A. Fukushima, et al., Appl. Phys. Express **4**, 063001 (2011).

[47] J. Zhang, T. Phung, A. Pushp, Y. Ferrante, J. Jeong, C. Rettner, B. P. Hughes, S.-H. Yang, Y. Jiang, and S. S. Parkin, Appl. Phys. Lett. **110**, 172403 (2017).

[48] C. J. Safranski, Y.-J. Chen, I. N. Krivorotov, and J. Z. Sun, Appl. Phys. Lett. **109**, 132408 (2016).

[49] T. Dohi, S. Kanai, F. Matsukura, and H. Ohno, Appl. Phys. Lett. **111**, 072403 (2017).

[50] T. Devolder, Phys. Rev. B **96**, 104413 (2017).